Optics & Laser Technology

Spatial tailoring of the refractive index in infrared glass-ceramic films enabled by direct laser writing

Check for updates

Ilya Mingareev[a,*], Myungkoo Kang[b], Mia Truman[c], Jun Qin[d], Gufan Yin[d], Juejun Hu[d], Casey M. Schwarz[c], Ian B. Murray[e], Martin C. Richardson[b], Kathleen A. Richardson[b]

[a] Department of Mechanical and Civil Engineering, Florida Institute of Technology, Melbourne, FL 32901, USA
[b] CREOL, College of Optics and Photonics, University of Central Florida, Orlando, FL 32816, USA
[c] Department of Physics and Astronomy, Ursinus College, Collegeville, PA 19426, USA
[d] Department of Materials Science and Engineering, Massachusetts Institute of Technology, Cambridge, MA 02139, USA
[e] BAE Systems, Nashua, NH 03064, USA

HIGHLIGHTS

- A photothermal process was employed to tune Ge-As-Pb-Se films' refractive indices.
- The index change was studied as a function of laser and heat treatment conditions.
- The index change is repeatable and scalable for films with thicknesses up to 40 μm.
- The study provides crucial guidance towards a gradient refractive index structure.

ARTICLE INFO

ABSTRACT

The development of infrared gradient refractive index (GRIN) components relies on the ability to modify the refractive index and dispersion properties of suitable host materials with a high spatial selectivity and a sufficient magnitude of change. We present a novel multi-step approach to induce local refractive index changes in chalcogenide optical materials. Films with thicknesses between 1 and 40 μm fabricated from multi-component $GeSe_2$-As_2Se_3-PbSe (GAP–Se) glass-ceramic materials were irradiated with continuous-wave and nanosecond-pulsed laser light, and post-processed with heat-treatments. A maximum local refractive index change of $\Delta n = 0.088$ across a broad spectral range in the infrared was realized. Spatial control of the refractive index variation was achieved through thermally-induced crystallization of a Pb-rich crystal phase. The magnitude of the index change scaled with the laser power and the exposure dose while the material maintained the required optical quality. The material performance validated in this study for thick films (20–40 μm films) reconfirms our ability to extend results from thin GAP-Se films towards novel optical designs.

1. Introduction

Steady progress in the design and development of broadband infrared (IR) sensor and beam delivery technology has led to an increased demand for suitable optical components and integrated systems that will meet high expectations in required optical resolution, compactness, and overall cost [1–4]. The limited performance of optical components made of homogeneous materials is often not sufficient for modern defense and commercial platforms, and the limited availability of commercially available IR optical materials can substantially limit the resulting design space. GRIN optics operating in the IR offer a possible solution to this challenge by featuring enhanced optical functionality and a significant reduction in size and cost, since glasses can provide advantages over commonly-employed crystalline substrates. Fabrication of IR GRIN optical systems is currently impeded by the limited availability of suitable host materials and manufacturing processes, since there is no commercially available method to allow precise three-dimensional (3D) tailoring of optical properties in the axial and radial directions with well-controlled and reproducible results.

Chalcogenide glasses (ChGs) are a class of optical materials featuring high transparency across a broad IR spectral range and the ability to tailor their refractive index through compositional variation

---

[4–11]. Recent studies have shown that the refractive index of selected ChG materials can be modified with high spatial selectivity through partial crystallization of the glass leading to formation of optical (glass-ceramic) nanocomposites. Experiments have demonstrated that the amount of crystallization or surface compositional change can be effectively controlled in 3D through the formation of nuclei and/or their growth within the ChG material by spatially-selective laser irradiation and heat treatment. Among other high-index ChG compositions, vapor phase deposited metastable thin-films of GAP-Se glasses [8–10] have shown the ability to modulate the refractive index through formation of high-index Pb-rich nanocrystals within the low-index glassy matrix. A comprehensive review of the state of the art in GRIN materials can be found in Ref. [4] along with the discussion of the potentials and limitations of various experimental methodologies and fabrication techniques.

In this study, we present a novel scalable approach to high-precision spatial tailoring of the refractive index in thin films produced from GAP-Se materials suitable for prospective IR GRIN components. A two-step photo-thermal process comprising irradiation of GAP-Se films in scanning patterns which exposes the material to precisely controlled optical intensities, and a subsequent heat treatment (HT) has been adopted to locally change the refractive index. We extend the results demonstrated for thin films of ChG (thickness $t \approx 1.1$ μm) to thicker ($t \approx 40$ μm) films. This experimental approach enables scaling-up of this technology towards the development of future component designs that require a large spatially defined refractive index change, Δn, over a more significant thickness to increase optical path difference (OPD) determined by the $t \times \Delta n$ product. Specifically, the key issues of interest in the present study include (1) confirmation of the ability to create thick, device-relevant GAP-Se films with uniform optical quality and compositional homogeneity (towards defining an upper limit of film thickness), (2) exploration of the photo-response for full-thickness exposure conditions near the film's absorption edge in pulsed and continuous-mode irradiation regimes, and (3) confirmation of repeatable post-exposure material response upon heat treatment leading to systematic energy dose-dependent refractive index evolution (and possible induced Δn saturation) within thicker films. In addition, we explore process parameter-property correlations to enable optimization of processing protocols for design and manufacture of IR GRIN optics. A comparison of the evolutionary nature of our efforts on GAP-Se (40 mol % PbSe) films to date is shown in Table 1.

Compared to the previous study utilizing 1064 nm pulsed laser light and large-area mask irradiation[9], we adopt here a direct laser writing (DLW) method that uses tightly focused nanosecond light at the wavelength $\lambda \approx 2$ μm that enables exposure of the complete film thickness. Combined with a beam scanning approach, this methodology potentially enables a complete 2D/3D processing selectivity needed for the fabrication of IR GRIN optics.

2. Experimental

2.1. Fabrication of infrared optical materials

Films of $15GeSe_2$-$45As_2Se_3$-$40PbSe$ were deposited onto Schott IRG 24 (Pb-free $Ge_{10}As_{40}Se_{50}$) substrates with diameters in the range 25–30 mm to evaluate maximum possible film thicknesses which could

be fabricated with compositional homogeneity and processed to realize index modification (Δn) throughout this thickness (t). The substrate was chosen to assure a close match in coefficient of thermal expansion (CTE) necessary to yield high-quality thick films. Thick films in the context of this work, are defined as glass layers thicker than 5 μm. Without adequate CTE match, such thick layers can exhibit crazing, wrinkling or complete delamination due to accumulated stress during the film deposition process. Prior to deposition, bulk target materials were ground to powder and loaded into two tantalum-baffled source boats. The films were deposited onto room temperature substrates in a thermal evaporator (112 Evaporator-Sputter Station from PVD Products Inc.) at a base pressure of 8×10^{-7} Torr. Deposition rates of the co-deposited target materials were stabilized at 20 Å/s for $GeSe_2$-$3As_2Se_3$ and 8.5 Å/s for PbSe, respectively following previously established protocols [12,13]. Subsequently, the films underwent a stress relieving anneal for 2 h at 145 °C under atmospheric pressure with N_2 carrier gas in a furnace (STF55666C from Thermo Scientific Lindberg). Fig. 1 shows top (a) and cross-sectional (b) views of various films upon deposition where the film layer is intact without any evidence of cracking or delamination. Maximum thickness of GAP-Se films realized to date (repeated over multiple deposition runs) is 40 μm. Thicker films have not yet been attempted. Likewise, we have not attempted to deposit the film on substrates with size larger diameters as suitable CTE-matched substrates were not available.

Transmission spectra were collected from uncoated (IRG 24) substrates and GAP-Se-coated substrates for different film thicknesses. Results show that the shortwave transmission cut-off edge of the as-deposited $t = 20$ μm film shown in Fig. 1 (c), is slightly red-shifted as compared to the underlying substrate. The apparent oscillations on the spectrum were due to the spectrometer not fully resolving the Fabry-Perot interference fringes resulting from reflections on front and back surfaces of the GAP-Se film and do not correlate with the film quality. This shift and the slight increase in Fresnel loss from the film's as-deposited refractive index (higher than the IRG 24), is attributed to the Pb contained in the glass film's composition. Lead is not present in the underlying substrate (GeAsSe). The transmission of the as-deposited, amorphous glass film thus requires use of an irradiation wavelength for laser processing longer than this edge. Selection of this wavelength is important to maximize the penetration depth of the incident laser beam while still being able to introduce microstructural modification to the complete film thickness. Previous efforts summarized in Table 1 have used 1064 nm nanosecond pulsed laser irradiation, where some film-induced absorption prevented transmission throughout the complete film thickness. This is not the case in the present effort as the $\lambda = 2$ μm laser light, with the irradiation conditions used, will fully penetrate the maximum layer thickness. In Fig. 1 (c), the as-deposited film remains transparent over a large range in the mid-wave infrared.

2.2. Laser irradiation process

Previous investigation of laser-induced modification of GAP-Se utilized continuous-wave (CW) radiation in the visible ($\lambda = 532$ nm) to physically heat bulk materials inducing crystallization [10] or near-infrared radiation in the pulsed (ns) mode [8,9] on thin films. While confirming the role of photon energy in these works and total cumulative laser dose required for laser-induced phase separation and

Table 1
Comparison of previously reported findings on GAP-Se films and the present work.

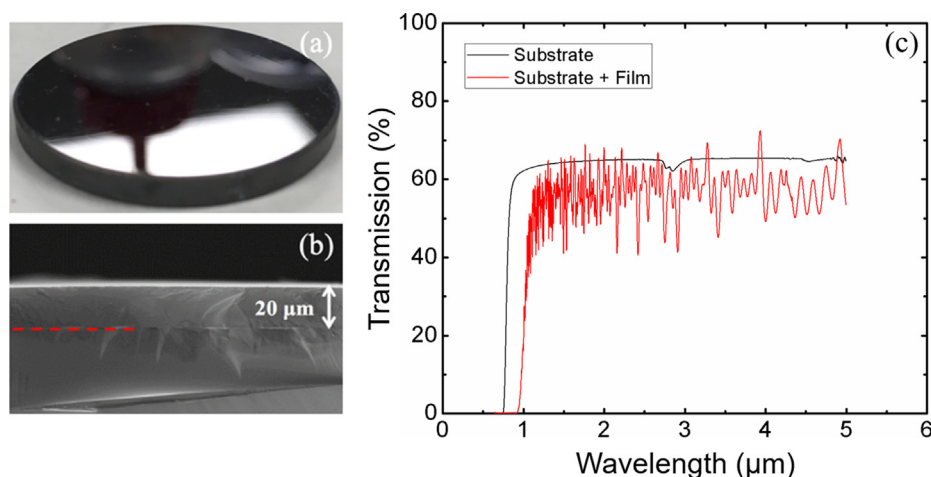| Film thickness (μm)	Laser exposure wavelength (μm)	Exposure regime	As-deposited film refractive index at $\lambda = 4.515$ μm	Reference
1.1	1.985	Pulsed: 100 ns/100 kHz	3.1380	This work
1.4	1.064	Pulsed: 10 or 20 ns/10 kHz	3.1408	[9]
1.1–25	1.985	Pulsed: 100 ns/100 kHz	20 μm: 3.1520	[15]
25	1.985	Pulsed: 100 ns/100 kHz	3.1529	[16]
20/40	1.985/1.970	Pulsed: 100 ns/100 kHz and CW	20 μm: 3.1520/40 μm: 3.1534	This work

Fig. 1. (a) Top-view of the 40 μm GAP-Se film on a 25 mm diameter IRG-24 substrate, (b) cross-sectional view of the sample showing the interface between the 20 μm GAP-Se film and the substrate, and (c) optical transmission of the t = 20 μm film, without correction for Fresnel losses.

subsequent crystallization, these wavelengths would not be suitable for transmission through the thick volumes of glass of interest in the present study. Thus, this effort utilized a fixed wavelength source compatible with the material's transmission edge (center wavelength, λ = 2 μm), in both a CW and pulsed mode to compare the mechanisms associated with photo-induced nucleation. In all cases, laser exposure was followed by an isothermal heat treatment protocol imparted to all regions (exposed and unexposed) of the sample.

A home-built thulium fiber laser that can operate either as a nanosecond Q-switch source or in continuous-wave mode with an emission wavelength of approximately λ = 2 μm was adopted in the experiments. At this wavelength, both the substrate and the GAP-Se film remain transparent. In pulsed mode, laser-induced modifications can be caused either by energy-cumulative effects due to linear or nonlinear absorption associated with high peak powers. In the CW mode, linear absorption is the main energy deposition process. Depending on the operation mode and the required output power level, the laser system utilizes a thulium fiber oscillator and one or two thulium fiber amplifier stages. Most nanosecond pulse irradiations of GAP-Se films were performed with the first amplifier stage of the master-oscillator-power amplifier (MOPA) system described in Ref. [14] and shown in Fig. 2. The laser output was linearly polarized, the beam diameter was expanded from initially 2.5 mm to approximately 4.5 mm, the beam quality was M^2 < 1.2, and the spectral width was < 1 nm (full width at half maximum, FWHM) at a variable wavelength between 1950 nm and 2010 nm. The pulse duration utilized in the study was adjustable in the range t_p = 100–200 ns, and the repetition rate was adjustable in the

range f_{rep} = 100–200 kHz. In order to operate the laser in CW mode, the Q-switch as well as additional pulse pickers and pulse cleaners based on acousto-optical modulators (AOM) were turned off. The output of the MOPA system was guided through a mechanical shutter (Uniblitz) to a vertical rail to achieve normal incidence of the beam onto the horizontally mounted targets. The beam was focused on the surface of the GAP-Se film to an approximate 15-μm spot size using an aberration-corrected triplet lens with a focal length f = 25 mm. The samples were mounted on a 3-axis motion controller stage (Newport VP-25X), while the lens was stationary.

Films were irradiated in 5 × 5 mm^2 square regions (pads) using line scan patterns at a constant translation speed of 1 mm/s and a line pitch of 50 μm, to avoid spatial overlap between adjacent lines. Both uniform large-area refractive index modifications and index step profiles can be implemented within a square by changing irradiation conditions used for individual lines. At a given line pitch, the energy deposition dose can be varied by adjusting three process parameters: (a) the output laser power, (b) the translation speed, and (c) the number of scans over the same area. In our experiments, the average laser power was varied in the range P = 30–400 mW and the number of scans was varied in the range N = 1–4, while all other parameters remained unchanged. As the total processing time of one square region is 500 s, the total dose, i.e. the optical energy provided but not necessarily absorbed at the target surface, can be calculated by multiplying the energy dose deposited per layer (laser power times 500 s) with the number of layers, N. All reported powers are "incident" values meaning that Fresnel reflections are not accounted for. For the 40 mol% PbSe GAP-Se films in the
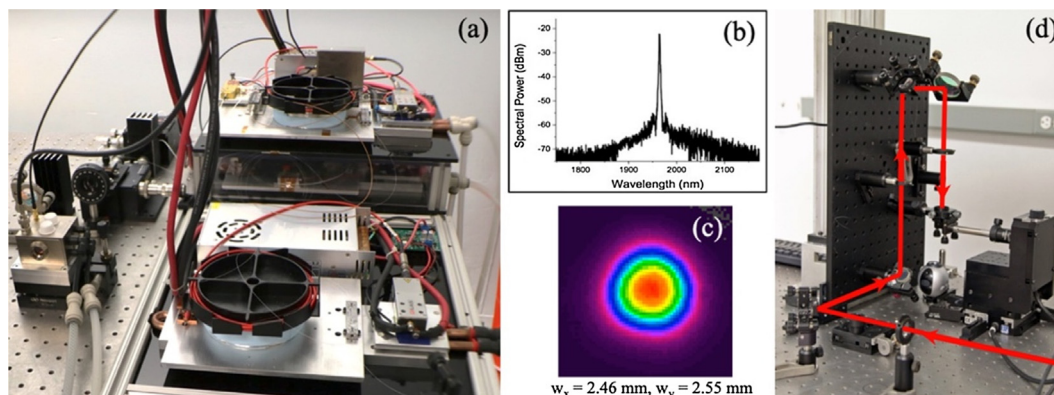

Fig. 2. (a) Image of the home-built Tm-fiber laser system, (b) optical emission spectrum in pulsed mode, (c) typical beam intensity distribution measured in far field, and (d) laser processing setup.
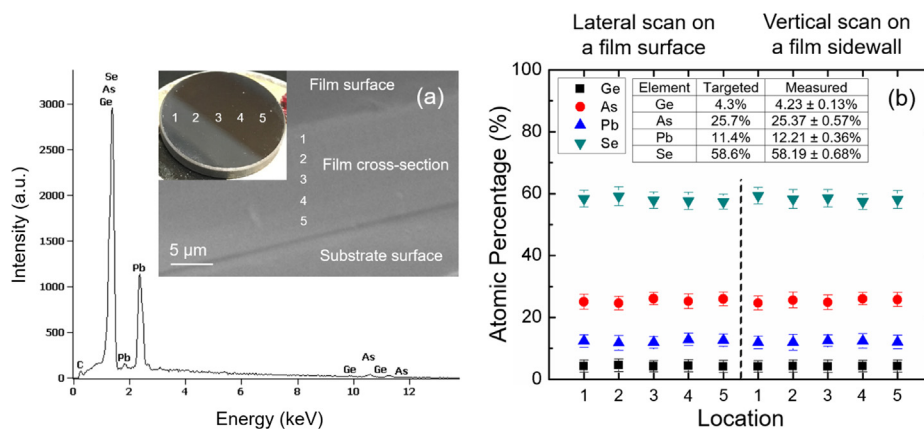
Fig. 3. (a) Example of the EDX spectrum obtained from the 20 μm thick film with locations of the measurements as shown by numbers (inset) for the 30 mm-diameter sample; (b) lateral/vertical compositional chart showing atomic percentages of constituents as measured in the position location shown in inset.

present study, (11 at% Pb) as-deposited glass films possess refractive indices of $n = 3.1522$ (for 20 μm films) and 3.1534 (for 40 μm films) at $\lambda = 4.515$ μm; this translates to ~70–75% transmission through the incident air/glass interface. For 10 kHz and 100 kHz pulsed regimes the pulse-to-pulse time is 100 μs and 10 μs, respectively. For this reason, it is likely that the 10–100 ns pulsed regime employed in these studies is well below that where ultra-short pulses at MHz-rates and nonlinear material response leads to heat/energy accumulation. Endeavors to study the nonlinear optical properties of these GAP-Se materials are in progress.

We have attempted to optimize the exposure conditions employed for this thick film study to ensure full film thickness, for complete volume irradiation. The lens used in the experiments produced an estimated spot size of 15 μm and a Rayleigh range of ~90 μm. This distance is for air; thus, in GAP-Se this number scales with refractive index, (i.e. for the base material index, the Rayleigh range would translate to > 270 μm). This means that even for 40 μm films the entire thickness of the film is irradiated at nearly constant dose along the (axial) propagation direction. This being said, we have no way of confirming if the laser-induced material modification resulting in the refractive index change is occurring in the entire film thickness concurrently, or if the film starts "responding" from top to bottom within the film thickness. As no in-situ imaging during processing is possible, we have assumed for our mechanistic explanation that the photo-response occurs simultaneously as we are measuring post-processed (overall) material modification. Subsequent depth-dependent assessment of post-exposure morphology (phase separation) and post-HT crystallization has to date (in films up to 20 μm thick) shown no evidence of gradients in crystal phase fractions as a function of depth. Thicker films (25 and 40 μm) are undergoing microscopic and x-ray diffraction analysis at present and will provide conclusive validation of the accuracy of this assumption.

2.3. Heat treatment protocol and material characterization

Upon laser irradiation, HTs were carried out in a muffle furnace (Thermo Scientific 48000) in air atmosphere calibrated with a type-K thermocouple that was placed next to the films on the same refractory brick. In the present study, three types of single-step heat treatment were conducted for the films. All HTs were performed at a temperature 190 °C for initially 30 min, 90 min and 180 min. For a limited set of measurements, the films were heat-treated for an additional 90 min at 190 °C yielding a total HT duration of 270 min. Films were visually investigated over an area of 1.6 × 1.6 mm^2 using white light interferometry (WLI, Zygo New View 6300) before and after heat treatment to determine and quantify the presence of photo- and/or thermal expansion upon laser irradiation and post heat treatment. Transmission spectra of the films were measured at wavelengths from 1.5 to 25 μm,

using a ThermoFisher Nicolet iS5 FTIR spectrometer. Room-temperature linear refractive indices of the films were measured at a wavelength of 4.515 μm, using a Metricon prism coupler modified for use in the infrared. Metricon measurement were performed utilizing the "knee" method where samples were in physical contact with a Si prism to identify an angle of internal reflection from the interface and accordingly correlate the angle to the index of the samples. All measured index values were through-plane refractive indices with a measurement error of $\Delta n \approx 0.0005$. Composition of the GAP-Se films was determined using energy-dispersive x-ray spectroscopy (EDX: Noran System 7 attached to a Zeiss Ultra-55 SEM). Cross-sectional transmission electron microscopy (TEM) specimens were prepared by ion milling followed by lift-out process in a FEI 200 TEM FIB. The specimens were then mounted on Cu grids and ion-polished to ~50 nm. TEM images were collected in FEI Tecnai F30 TEM.

3. Discussion of results

3.1. Characterization of the film compositions

Compositional uniformity of thermally evaporated GAP-Se films is key to successful implementation of spatially selective refractive index change using the proposed scanning laser beam approach. Homogenous film composition in thick thermally evaporated films is often a challenge in materials where the thermal history of the film at the near-substrate surface can be different from that of the film surface far from that interface where the underlying film can be heated from deposition-induced 'energy'. This effect can be exacerbated in very thick films such as those in the present effort. Such energetics can also lead to film volatilization in the case of films where multiple constituents exhibit varied or preferential evaporation behavior resulting in thickness-dependent film property variation. Shown here is the *lack* of these effects, mitigated by specific deposition process optimization. Results of the compositional homogeneity characterization for a 20 μm thick GAP-Se film are shown in Fig. 3. As depicted in the EDX data shown, measurements were performed at 5 different (radial) locations across the film surface and at 5 different (axial) locations along the cross-section of the film specimen's depth. The results show that the atomic percentages of the main chemical constituents Ge, As, Pb and Se are within the ± 0.13%, ± 0.57%, ± 0.36% and ± 0.68% tolerance ranges, respectively and is considered compositionally uniform throughout the specimen geometry. Similar results have been realized for other film thicknesses [15,16] illustrating the robustness of the film deposition protocol employed to minimize compositional, stress and thermal history variation during a thick film deposition.

3.2. Characterization of the laser-induced surface morphology changes

Laser modification thresholds for GAP-Se films were first determined for pulsed and CW emission modes. Films of various thicknesses were processed by inducing line modifications on film surfaces at varying pulse energies, while keeping all other process parameters constant, (i.e., the translation speed set to $v = 1$ mm/s and the pulse repetition rate set to $f_{rep} = 100$ kHz). Initially, average power between lines was increased in increments of 10 mW until visible macroscopic modification occurred in the film. The experiment was repeated with an increment of 2 mW in a narrower interval of average power around the assumed modification threshold value, P_{thr}. Post-exposure surface modifications were then investigated using optical microscopy, including WLI. With increasing laser power, the onset of damage often occurred at pre-existing surface imperfections such as micro-scratches and other surface irregularities, referred to as damage accumulation [17]. At higher powers and in the absence of visible pre-existing imperfections, the surface film morphology exhibited negligible photoexpansion due to local heating. In these cases of GAP-Se film exposure, no ablation or trench formation was observed. Lastly, at even higher laser powers, film ablation through evaporation and melt ejection occurred. Here, however, while imparting visible damage, no visible film delamination due to laser processing was observed. In films of all thicknesses, initial film modification in the pulsed regime occurred at approximately $P_{thr} = 185$ mW (1.85 µJ in terms of pulse energy), which defined the power threshold value not to be exceeded in subsequent irradiation experiments. In the CW mode, no visible ablation was detected (even at sites with microscopically visible imperfections) below the maximum adopted power of 400 mW. Above this level some modification was occasionally observed. Thus, this defined the upper power level of our CW exposure protocol.

Large-area laser irradiation pads were created to verify spatial uniformity and response of the thick films and to assess local variation in physical and optical properties for defined writing (and subsequent heat treatment) conditions. Here, evaluation of post-photo-induced material expansion or other surface morphology changes due to repetitive pulsed surface irradiation and/or possible damage accumulation was inspected using white light interferometry (WLI). Surface roughness (RMS) was measured in films irradiated under different conditions, and exposed pad areas (nominally 5×5 mm^2) were compared to unexposed reference regions. Measurements were performed in multiple series at various locations along the surface area, and The exemplary results obtained from different sample areas (Fig. 4) show that the RMS surface roughness of the most intensively irradiated region ($P = 400$ mW, CW irradiation regime) remains similar to that of the pristine reference (unexposed) region [Fig. 4(a)], thus indicating that photo-expansion is low or negligible under the irradiation conditions selected [Fig. 4(b)]. Additionally, no further expansion in irradiated squares was observed following post-exposure heat treatment [Fig. 4(c)].

3.3. Refractive index changes

The compositional homogeneity conclusions shown in Fig. 3 represent an important starting point confirming the glass' ability to be converted *uniformly* via the photo-exposure/heat-treatment protocol required for GRIN fabrication, when carried out at various spatial positions upon irradiation. Demonstration of repeatable compositional uniformity realized through the controlled deposition protocols employed across films of various thicknesses confirms repeatability of starting material behavior. This enables spatial variation of laser irradiation to be the 'knob' that dictates the local dose the glass film sees, to 'nucleate' the subsequent phase transition (crystallization) realized upon HT. Irradiation dose is defined by the laser wavelength, total photon dose (pulsed or CW) and focal conditions (defining the localized focal position within the film) where modification is initiated and

subsequently occurs via post-heat treatment crystallization. As noted above, our goal has been to *homogeneously expose* macroscopic pads of the film's full thickness, followed by a *homogeneous HT* to convert exposed regions. This process results in an array of dose-dependent pads of glass ceramic possessing effective refractive index (n_{eff}) changes proportional to the resulting relative fractions of induced crystal phases and residual glass phase. Such a strategy could be extended to other geometries, whereby dose can be varied spatially to create a *continuous gradient* in extent of post-exposed crystallization and effective index change.

Comparing resulting material response to irradiation with pulsed and CW laser light is another important aspect of this study. It is assumed that high peak powers up to several tens of watts available in the nanosecond pulsed mode, could induce qualitatively different modification behavior compared to irradiation in CW mode, and affect the magnitude of the achievable local refractive index. On the other hand, it is known that processing semi-transparent materials with short laser pulses enables a greater degree of spatial energy deposition control, which could potentially extend the design space of future GRIN devices from 2D for thin films, to 3D for thicker films and even bulk materials. Pulsed and CW exposure conditions in this study were directly compared when irradiating homogenous films. To estimate the accumulated energy dose, the (average) power multiplied with the total processing time of 500 s per 5×5 mm^2 pad was used in both irradiation regimes. For example, the lowest energy dose applied in this study was 15 J with the corresponding accumulated energy density of 60 J/cm^2 for pulsed irradiation at 30 mW, whereas the highest energy dose was 200 J with the accumulated energy density of 800 J/cm^2 for CW irradiation at 400 mW. For multi-scan irradiation, the single-scan energy dose was multiplied with the number of scans N. Irradiation with 100 ns nanosecond laser pulses resulted in single-pulse peak powers in the range 3–15 W, and single-pulse irradiances in the range 1.7–8.5 MW/cm^2. Quantitative analysis of nonlinear absorption and the material response is currently underway. In addition, no effects of spatial overlap between pulses and the scanning pattern on the resulting local refractive index distribution were studied, and instead the refractive index change (compared to the unexposed materials) averaged over of the entire pad area was analyzed.

Compositionally homogeneous films of two thicknesses (20 µm/pulsed and 40 µm/pulsed and CW) were irradiated in 5×5 mm^2 patterns. For pulsed irradiation, the average power was varied in the range $P = 30$–150 mW, limited by the onset of surface ablation at approximately 180 mW. For CW irradiation, the laser power was varied in the range $P = 60$–400 mW. In both irradiation regimes the number of scans was varied from 1 to 4. Multiple scans (N) were investigated to evaluate the role of scan number needed to realize the maximum extent of nucleation (defined by transition from a homogeneous glass to a compositionally-segregated, phase separated amorphous film). This full extent of nucleation is desirable to ensure maximum diffusion of the Pb species into Pb-rich regions which participate post-HT in the formation of high refractive index Pb-containing nanocrystals. For each set of the process parameters adopted in laser experiments, the refractive index was measured following laser exposure before HT and after 30, 90, 180, and 270 min of HT. In all cases, un-irradiated regions adjacent to the patterned squares were measured to confirm HT (with no laser exposure) did not induce any index modification.

Fig. 5 illustrates post-exposure plus heat-treatment refractive index change in 20 and 40 µm thick films. Fig. 5(a) shows the refractive index change in the 20 µm film where the combined pulsed laser irradiation and post heat treatment processing resulted in a maximum index increase of $\Delta n \approx 0.072$ for the pattern irradiated at 150 mW (1 scan) and heat-treated for 180 min. This corresponds to an accumulated dose of 300 J/cm^2. Comparing similar pulse regime modification of the 20 µm film for higher dose at lower power, a total index increase of $\Delta n \approx 0.051$ for the scan region irradiated at 60 mW (2 scans) was observed after the same heat treatment time. The accumulated dose for
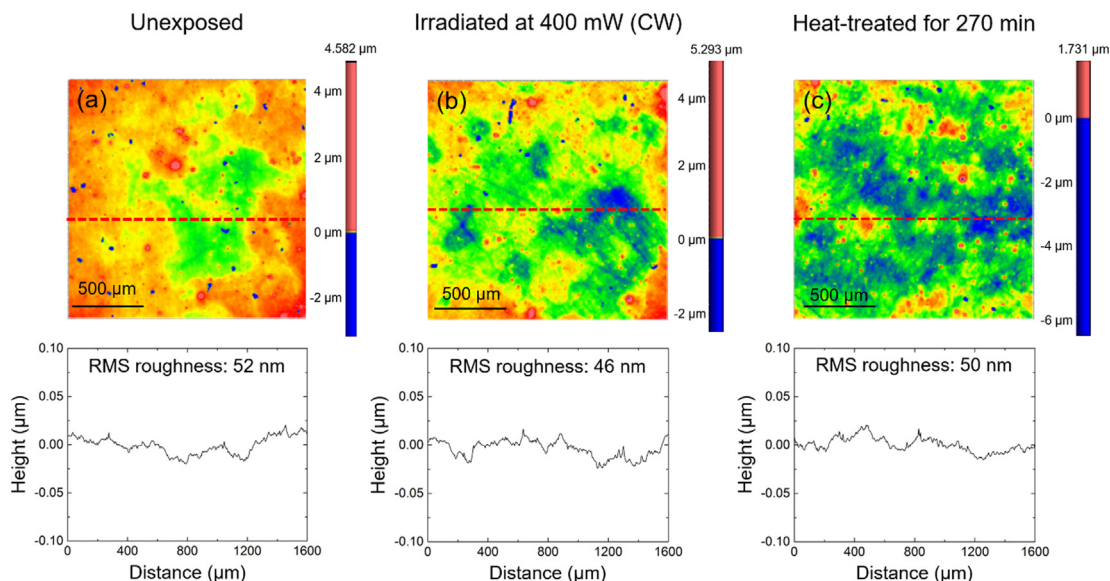
Fig. 4. Results of surface morphology evolution for a $t = 40$ μm GAP-Se film. Shown for unexposed (a), post-exposed (CW irradiated, $P = 400$ mW) (b), and a subsequently heat-treated film (c). The typical areas shown have dimensions of 1.6×1.6 mm^2, and the RMS linear height profiles were extracted from red horizontal lines shown in each Zygo WLI image.

this exposure is 240 J/cm^2. As can be observed in the index change evolution in Fig. 5(a), the index increase has to date not yielded evidence of saturation for the maximum index at exposure/heat treatment time at 150 mW/180 min. This suggests that additional Pb in the glass matrix, while participating in the laser-induced segregation step, remains available for subsequent conversion into Pb-containing crystallites.

Fig. 5(b) shows the results obtained for the 40 μm film irradiated in pulsed and CW modes. Several important conclusions can be drawn from the data shown in the photo-response (with post heat treatment) of this much thicker film. First, the magnitude of maximum refractive index increase of $\Delta n \approx 0.088$ was realized for the scan region irradiated at 300 mW (1 scan) after 270 min of heat treatment. Irradiation of the 40 μm film at even higher laser power of 400 mW resulted in a slight reduction of the refractive index (by $\Delta n \approx 0.0010 \pm 0.0005$) compared to the index obtained at 300 mW, which is suggestive of a possible 'depletion' of crystallizable species. Second, as shown by the dashed boxes comparing 60 mW (2 scans) and 150 mW (1 scan) pads in Fig. 5(a) and (b), these exposures in the same pulsed mode result in nearly the same magnitude of induced index modification after same

heat treatment condition. These results suggest that both irradiation regimes activate creation (phase separation upon exposure) and subsequent conversion (crystallization) of the Pb-rich phase, highlighting film thickness-independent repeatability of index modification under identical laser exposure *dose* and post heat treatment time. This uniformity suggests that the optimized deposition protocol imparted to control thermal history of the glass during deposition to ensure low stress and compositional uniformity for thicker films yields successful index repeatability and a lack of film delamination. Index repeatability here is demonstrated both in the index stability obtained from the unirradiated regions (pre- and post-HT), and consistently similar index values obtained from irradiated regions without any heat treatments (green diamonds). Third, it is also important to note that, as evidenced by two dashed boxes in Fig. 5(b), pulsed and CW modes at the same power and scan number result in nearly the same magnitude of induced index modification after same heat treatment condition.

It should be noted that the repeatability and reproducibility of the presented index tailoring approach is not determined entirely by the index measurement error of $\Delta n \approx 0.0005$, but depends on a number of process related factors such as the device-specific process parameter
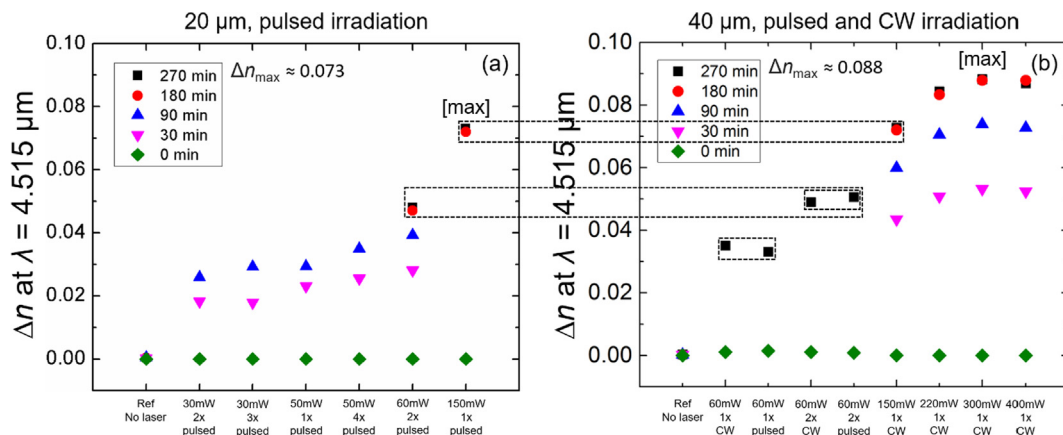

Fig. 5. Refractive index change (measured at $\lambda = 4.515$ μm) as a function of average laser powers and scan numbers for different heat treatment time. (a) 20 μm film irradiated with nanosecond (ns) pulses. (b) 40 μm film irradiated in (ns) pulsed and continuous-wave (CW) modes. The dashed box across the two figures are a guide to the eye highlighting film thickness-independent repeatability of index modification under identical laser exposure dose and post heat treatment time. The two dashed boxes inside (b) are drawn to compare pulsed and CW modes at the same power and scan number to show similarity.
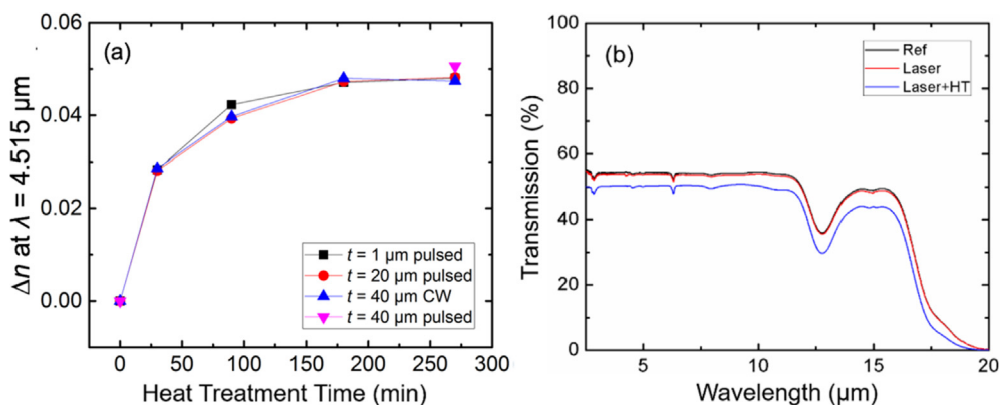
Fig. 6. (a) The change in refractive index measured at different heat treatment times at λ = 4.515 µm for varying film thicknesses following 60 mW (2 scans) irradiation and heat treatment at 190 °C. Error bars are within the data point. (b) Optical transmission (not corrected for Fresnel loss) of the 40 µm thick film as-deposited, after CW exposure (laser) and after heat treatment for 270 min (laser + HT).

uncertainties both for laser irradiation and heat treatment processes. Considering possible process parameter variations occurring during these processes, we estimate the process induced error in refractive index determination to be < 2% for irradiation at higher laser powers > 100 mW, and < 1% otherwise.

Summarizing the index increase as a function of heat treatment time for regions exposed to constant exposure power for the two films examined here (in pulse and CW modes respectively) and prior results on 1 µm films (pulsed mode) provides insight into the mechanistic changes believed to be taking place in the laser modification of GAP-Se films. In Fig. 6(a), the total induced index change for up to 270 min heat treatment of each film following pulsed and continuous wave irradiation is shown. For every heat treatment timestep, the change in refractive index for each film is similar, implying index modification reproducibility. Next, while all films are confirmed (Fig. 3 and prior measurements on other film thicknesses) to possess identical concentrations of Pb and thus have the same total Pb ions available to participate in formation of Pb-rich nanocrystals, the cumulative volume fraction of ions over the film's depth will be related to the fractional separation into Pb-rich phases induced by irradiation. As the irradiation conditions used subjects the full film depth (and thus volume) for each film shown, the resulting refractive index will evolve as these Pb-rich amorphous regions convert to form higher index nanocrystals. Here, further HT (time) leads to growth of a higher volume fraction of higher-index crystal phase(s), concurrently reducing the volume fraction of lower-index residual glass matrix thus defining the resulting n_{eff} of the nanocomposite in the irradiated region. This conversion process occurs over the full glass thickness, and while the Metricon refractometer cannot measure the full thickness of the film, the conversion resulting in the index change for both bulk and thin film specimens (discussed below), has been documented via electron microscopy. All films exhibit

evidence of index increase saturation suggesting that only minimal further index increase is possible with further heat treatment. This again suggests that the conversion to Pb-rich nanocrystallites is nearly complete, initiated by irradiation but limited by the available species for crystallization and the period of time for growth.

While the refractive index change is significant, no appreciable degradation in film transmission is observed, suggesting any processing-induced scattering is minimal. Additionally, no apparent volume change is seen between the modified pad regions and the surrounding unexposed regions of the pads, indicating that the extreme stepwise index change does not result in a change of surface topology that could lead to optical distortion. Crystallite sizes in 40 µm films are sub-50 nm in size. Hence the transmission seen for the base, laser-exposed and laser plus heat-treated films in Fig. 6(b) only shows transmission reduction associated with the film's index increase. Data shown here have not been corrected for Fresnel loss. Maintaining optical properties such as the sufficient transmission is essential for the performance of the GRIN optics. Therefore, in addition to determining the refractive index change induced by exposure plus heat treatment, the fact that minimal degradation to optical transmission of the film is observed is promising for use of these materials in both the mid- and longwave spectral regimes.

The thickness-independent index modification uniformity is cross-confirmed by resulting microstructures upon laser and post heat treatment. Fig. 7 shows dark field TEM images collected from films with thicknesses of 1.4, 20, and 40 µm which underwent pulsed (1.4 and 20 µm) and CW (40 µm) laser irradiation and the same post heat treatment condition (180 min at 190 °C). It is evident that the size (< 50 nm), volume fraction, and connectivity of the bright Pb-rich crystalline phases, which give rise to index modification, are very similar throughout all cases. Specifically, the index increase is attributed
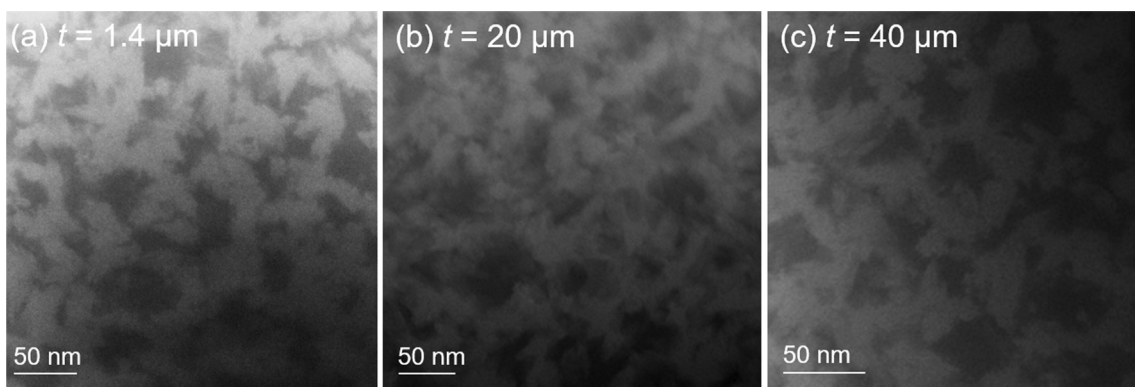

Fig. 7. Dark-field cross-sectional TEM images of films with thicknesses of (a) t = 1.4 µm, (b) t = 20 µm, and (c) t = 40 µm. Co-existing Pb-rich, high-index, crystalline phases (bright) and a Pb-deficient, low-index, amorphous phase (dark) can be shown in each image, as well as the consistency of their size and distribution between images. This provides evidence for scalability, as the thickness of the film does not factor into index modification results.

to the generation of high-index crystallites co-existing with a relatively low-index (Pb-depleted) glassy phase. Three primary crystalline phases including PbSe, As_2Se_3, and Se crystals have been identified to be formed upon laser exposure and post heat treatment [9,16]. Among the phases, PbSe has a refractive index of ~4.9 which is far greater than that of the base film's refractive index of ~3.12. Thus, the high-index Pb-containing crystalline phase increases the effective index of the resulting glass-ceramic nanocomposite films with respect to that of the initial base glass films. As noted above, the atomic concentration of Pb present in the base glass films dictates the volume fraction of the high-index Pb-containing crystallites that can form, which in turn dictates the extent of resulting index modification upon crystal growth with heat treatment. Since the nominal composition of the three films with thicknesses of 1.4, 20, and 40 μm shown in Fig. 7 is identical, the resulting volume fraction of high-index crystalline phases and index changes are likewise believed to be identical. This validates our assumption that the mechanism seen in thin films can be extended to thick films, with sufficient attention to illumination conditions (laser dose and focusing conditions). It also demonstrates the scalability of our photo-thermal process, microstructural evolution, and index modification to a wide range of film thicknesses.

3.4. Implication of results on thick GAP-Se films irradiated in pulsed and CW modes

Experimental results confirm that for both pulsed and CW laser exposure of the thick GAP-Se films investigated in this study, films follow the previously reported mechanism for induced index change seen in much thinner GAP-Se films. It has been shown that the film's refractive index only increases as a result of laser exposure conditions (defining the Pb-rich phase formation) and the subsequent extent of crystal growth during the heat treatment time. As presented above, film exposure to high-intensity laser light leads to phase separation of the initially homogeneous glass film into Pb-rich and Pb-deficient amorphous phases. Upon film exposure these two phases are still glassy (amorphous), and the measured effective index of the nanocomposite following exposure *only*, remains largely unchanged. Once heat treatment is performed at a temperature between approximately 150 and 200 °C, the Pb-rich phases will crystallize resulting in a high-refractive-index phases in the surrounding low-index glassy Pb-depleted matrix. The upper temperature limit for the specific composition (200 °C here) corresponds to the temperature where unexposed material starts to spontaneously crystallize, leading to uncontrolled crystal growth and subsequent optical transmission degradation (primarily scatter loss). HTs below this spontaneous crystallization threshold results in the increase of the effective index of the glass-ceramic nanocomposite solely within the Pb-rich amorphous phase due to its reduced glass stability. This then enables the spatially localized formation of high-index crystals only where exposure has previously occurred. Thick films in the present study exhibited this same mechanism, consistent with findings realized for *thin* 1 μm films of the same composition [9]. A loss of this spatial processing selectivity reduces film transmission for treatment above the threshold temperature making fabrication of custom GRIN profiles impossible. These results confirm that refractive index change is determined by the combined photo-thermal dose effect, i.e. the magnitude of the refractive index depends both on the laser exposure dose, and the duration of the subsequent heat treatment that controls the crystallization process, for homogeneous composition films ranging from 1 to 40 μm in thicknesses.

As previously mentioned, while longer HT times (up to 180 min) generally resulted in larger degree of crystallization of the Pb-rich phase, additional heat treatment time up to a total duration of 270 min did not lead to an appreciable further increase in index suggesting the point of ultimate saturation. This was confirmed both in pulsed and CW irradiation modes, as shown in Figs. 5 and 6. For each photo-exposed region, the index increases with increasing HT time until the high-index

crystalline phase and, consequently, the effective refractive index are quasi-saturated. This is likely a limit that is due to the finite amount of compositional species available to participate in the higher index crystallite phase formation and crystallization process. An accurate correlation between the crystallization behavior for different glass phase and constituents (i.e. Ge, As, Pb and Se) and the index change cannot be determined at this point, and further studies into the phase evolution in GAP-Se materials exposed to intense laser light are currently underway.

The effects of the laser exposure dose and other irradiation conditions on the resulting maximum index change are manifold. A comprehensive review of photo-induced phenomena in chalcogenide glasses is given in Ref. [18]. Three distinct modification regimes of ChG materials have been identified in the literature: (1) non-thermal modification, including photo-crystallization and photo-darkening, (2) anisotropic modifications induced by polarized light, and (c) modifications caused by non-linearities in light-matter interactions. In this work, we aimed to explore differences in material modification behavior based primarily on the temporal excitation regime and energy dose considerations. The amount of optical energy absorbed in the film may vary as a function of the laser power, temporal irradiation mode, i.e. pulsed versus CW, the existence of one or several material modification thresholds, linear and non-linear absorption properties, and the compositional phase evolution of the material. On the one hand, the results indicate there is a direct, nearly linear correlation between the utilized CW laser power (or average laser power for pulsed mode) and the resultant Δn for powers up to 60 mW. For example, irradiation at 30 mW (Fig. 5a) in pulsed mode leads to an index increase of approximately 0.025 compared to unexposed material, while doubling the laser power to 60 mW results in $\Delta n \approx 0.049$. This illustrates a nearly linear increase, while keeping all other process conditions constant. At larger applied powers, i.e. > 60 mW, the refractive index increase begins to saturate. This is regardless of pulsed or CW irradiation. For example, CW irradiation at powers greater 220 mW produced a nearly constant level of refractive index change in the 40 μm film. The laser power-related saturation seen for CW exposure, likely associated with some form of accumulation, was not observed for films processed with pulsed irradiation. In these exposures the highest adopted average power was 150 mW. Higher power exposure resulted in damage to the material at powers > 180 mW, a level not believed to be the intrinsic limit, rather likely due to surface imperfections. On the other hand, processing of films in several layers ($N > 1$) at a constant power indicates that the cumulative energy effect is not prominent, e.g. doubling the number of layers does not result in the corresponding increase of the refractive index. This suggests that the available species for subsequent crystallization (i.e., the Pb-rich amorphous phase created by irradiation), is largely realized in a 'single' layer of exposure as shown in the 'net' index change measured in Fig. 5a and b for similar irradiation powers.

In conventional laser machining of opaque and semi-transparent materials using CW and pulsed laser light, substantial qualitative differences are expected in the overall material modification behavior and the resulting morphology changes. When using irradiation in pulsed mode, materials can be processed with higher spatial accuracy without affecting larger material volumes surrounding the laser-matter interaction site, resulting effectively in better energy deposition control compared to the CW mode. In our pulsed irradiation experiments, peak powers on the order of several tens of Watts (for 100 ns pulses) were adopted, however the laser beam was focused fairly loosely, which prevented high optical intensities from occurring in the focal area. The refractive index and surface morphology data obtained for the pulsed mode did not indicate that the high peak powers caused a qualitatively different material modification. In fact, a direct comparison of the relative index change for the pulsed and CW modes illustrates very similar results for a given value of the (average) power. It should be noted however that no spatially resolved index measurements were performed in this work, and no experimental data was collected that

would allow studying the index distribution on microscale, including, as a function of film depth. As noted, the extent of depth that the Metricon system probes and thus can measure, is not indicative of the cumulative optical path difference created by the product of the film's thickness and its magnitude of index modification (Δn).

Given that the cumulative effects for $N > 1$ do not appear to play a significant role in increasing the refractive index change, it can be assumed that the intensity of the electro-magnetic field created on the film's surface during the laser-matter interaction, and not the total accumulated energy, is the primary factor responsible for the processing efficiency. The effects of nanosecond laser exposure mode on the effective index change should be further investigated to study possible impacts of non-linear (e.g. multi-photon) absorption. Despite the relatively high non-linear refractive index of GAP-Se on the order of 10^{-6} cm^2/GW [6], it is assumed that pulse peak powers on the order of kW and higher, combined with tighter focusing, will be needed to initiate effective multi-photon absorption at focusing conditions adopted in this work. Such irradiation conditions will be required to now exploit the 'real estate' now enabled by the availability of film thicknesses, where discrete exposure volumes as a function of depth, will enable discrete regions of spatially varying refractive index modification enabling axial GRIN structures.

The use of even shorter IR laser pulses (e.g. with picosecond or femtosecond pulse durations) for index tailoring may be considered to further extend the process limits, i.e. to increase the magnitude of the local refractive index and to improve the spatial processing selectivity. Our group has previously studied the processability of various semiconductors and other infrared materials using DLW in ultrashort regime [19]. The results have shown that due to the high intensities inherent to ultrashort pulses, near-critical electron densities may be created near the laser-incident surface causing an increase in local absorption and blocking light propagation into the volume of the material. Therefore, DLW with longer laser pulses is considered more suitable for in-volume processing of infrared materials [20].

3.5. Design considerations for infrared GRIN optics

In order to evaluate the performance of future GRIN optics produced with the method presented here, it is necessary to estimate the maximum optical path difference (OPD) that can be realized in GAP-Se films in the infrared. The highest refractive index change (0.088) obtained to date in 40 μm films will create an effective OPD = 3.52 μm (or approx. 0.78λ for the wavelength λ = 4.5 μm) compared to the unexposed material. While this work focused on forming discrete refractive index steps define in our exposed pads, the range of exposure conditions (if made in a rotationally-symmetric pattern, for example), would allow the fabrication of a radial GRIN layer on a lens to create aspheric performance from a spherical surface, based on knowledge of laser dose delivery and post-HT index change. Likewise, a sufficiently thick layer could create an axial GRIN to increase or decrease the effective focal length of an optical element, and by combining these techniques, this method could create true 3D index modification that would significantly decrease the overall number of optical elements in the system. The ability to tailor the index change in the film plane enables fabrication of gratings and other gradient index distributions; the contrast in Δn between the exposed and unexposed regions dictated by the film's composition will ultimately define the spatial resolution of these distributions. The use of the short pulse exposure mode will potentially enable another route to customizing index distributions in these and thicker GAP-Se films. By utilizing tightly focused nanosecond pulsed laser light, a high spatial selectivity not only in the lateral dimension, but also in axial directions will be facilitated, resulting in full 3D control of the film's refractive properties. Our estimations based on simulation of beam propagation [21] show that refractive index changes can be induced in several independent layers in 40 μm GAP-Se films when using high-NA focusing optics and high-intensity nanosecond pulsed

laser light.

4. Conclusions

GAP-Se films with thicknesses ranging from approximately 20 μm to 40 μm have been exposed to high-intensity nanosecond and continuous-wave laser light and heat-treated to evaluate local refractive index change due to selective crystallization of lead-rich amorphous phases. Laser irradiation was performed using a home-built Tm-doped fiber laser operating at the wavelength 2 μm, which enables spatially selective processing of GAP-Se with high penetration depth without inducing damage to the film and/or the underlying, CTE-matched chalcogenide glass substrate. Compositional analysis confirmed that an optimized deposition protocol specifically designed to minimize heating and thus stress during deposition, resulted in thick films (up to 40 μm thick) with superb chemical homogeneity. Several series of direct laser writing and heat treatment experiments were performed to (a) identify laser damage and/or modification thresholds of the materials, (b) produce 5×5 mm^2 irradiated line patterns by varying the laser power and the cumulative energy dose, and (c) study the effect of heat treatments on the resulting local refractive index. Results show that the maximum index increase of $\Delta n \approx 0.088$ was determined in scan areas irradiated at the average power of 300 mW, and following 270 min of isothermal heat treatment at 190 °C. While CW exposure for the composition and film thicknesses studied here appear to saturate, pulsed (ns) exposure shows no saturation, but will be limited by film surface quality impacting laser induced damage at the entrance surface.

Analysis of post-processed parts confirm that the photo-thermal protocol, employed for thin glass films and previously reported, can be extended to thick films more suitable for GRIN applications. A maximum possible OPD of 0.78λ (at 4.5 μm) has been realized for the index increase quantified for the thickest films evaluated to date, which is sufficient to create meaningful system performance enhancements as a radial GRIN layer on a lens. An upper limit to possible film thickness possible using the optimized deposition procedure has not been realized. It has been confirmed that our proposed laser-induced phase separation/HT induced crystallization mechanism resulting in effective index modification, applies to films with increasing film thickness, as long as the composition remains homogeneous throughout the film. Correlation of the induced phases, phase fractions and size distribution of nanocrystals, and their impact on the resulting index and dispersion is in progress. Dispersion modification, also a key attribute required in the optical design of structures based on such media, will also vary with heat treatment of the resulting modified regions and will be reported in a subsequent publication [22]. These data taken together show meaningful promise towards enhanced tailorability of key optical functionality. The study shows that the presented direct-write method can be applied to selective index patterning of even thicker GAP-Se films not only in 2D, but also lends itself to use in 3D structures.

It should be noted that while the presented hybrid photothermal process was demonstrated for Ge-As-Pb-Se chalcogenide materials, the process can be applied to a wide range of infrared materials where high refractive index phases can be systematically formed and grown by such external energetic stimulation to increase the overall index of the resulting nanocomposite while maintaining their sub-wavelength size to keep the nanocomposite optically transparent.

CRediT authorship contribution statement

Ilya Mingareev: Writing - original draft, Methodology, Investigation. **Myungkoo Kang:** Writing - review & editing, Data curation, Investigation. **Mia Truman:** Methodology. **Jun Qin:** Resources. **Gufan Yin:** Resources. **Juejun Hu:** Writing - review & editing, Resources. **Casey M. Schwarz:** Writing - review & editing. **Ian B. Murray:** Writing - review & editing, Resources. **Martin C. Richardson:** Resources. **Kathleen A. Richardson:** Writing - review &

editing, Project administration.

Declaration of Competing Interest

The authors declare that they have no known competing financial interests or personal relationships that could have appeared to influence the work reported in this paper.

Acknowledgments

References

[1] D. Gibson, S. Bayya, V. Nguyen, J. Sanghera, M. Kotov, C. McClain, J. Deegan, G. Lindberg, J. Vizgaitis, IR GRIN optics: design and fabrication, Proc. SPIE 10181 (2017) 101810B.

[2] Y.J. Tsai, S. Larouche, T. Tyler, G. Lipworth, N.M. Jokerst, D.R. Smith, Design and fabrication of a metamaterial gradient index diffraction grating at infrared wavelengths, Opt. Express 19 (2011) 24411.

[3] D. Gibson, S. Bayya, V. Nguyen, J. Sanghera, M. Kotov, G. Drake, GRIN optics for multispectral infrared imaging, Proc. SPIE 9451 (2015) 94511P.

[4] K. Richardson, M. Kang, L. Sisken, A. Yadav, C. Blanco, M. Antia, S. Novak, B. Gleason, C. Smith, A. Buff, A. Lepicard, M. Dussauze, C. Schwarz, S. Kuebler, C. Grabill, C. Pantano, T. Mayer, A. Pogrebnyakov, C. Rivero-Baleine, A. Kirk, S. Mensah, M. Driggers, J. Hu, P.-T. Lin, A. Agarwal, C. Li, W. Deng, Advances in infrared GRIN: a review of novel materials towards components and devices, Proc. SPIE 10627 (2018) 106270A.

[5] S. Novak, P.T. Lin, C. Li, C. Lumdee, J. Hu, A. Agarwal, K. Richardson, Direct printing of multilayer gradient refractive index chalcogenide glass coatings by electrospray, ACS Appl. Mater. Interfaces 9 (2017) 26990.

[6] K. Richardson, A. Buff, C. Smith, L. Sisken, J.D. Musgraves, P. Wachtel, T. Mayer, A. Swisher, A. Pogrebnyakov, M. Kang, C. Pantano, D. Werner, A. Kirk, S. Aiken, C. Rivero-Baleine, Engineering novel infrared glass ceramics for advanced optical solutions, Proc. SPIE 9822 (2016) 982205.

[7] A. Yadav, A. Buff, M. Kang, L. Sisken, C. Smith, J. Lonergan, C. Blanco, M. Antia, M. Driggers, A. Kirk, C. Rivero-Baleine, T. Mayer, A. Swisher, A. Pogrebnyakov, A.R. Hilton, G. Whaley, T.J. Loretz, A. Yee, G. Schmidt, D. Moore, K. Richardson, Melt size dependent property variation in GeSe$_2$-As$_2$Se$_3$-PbSe (GAP-Se) glass ceramics for infrared GRIN applications, Int. J. Appl. Glass Sci. 10 (2019) 27.

[8] M. Kang, L. Sisken, J. Cook, C. Blanco, M.C. Richardson, I. Mingareev, K. Richardson, Refractive index patterning of infrared glass ceramics through laser-induced vitrification, Opt. Mater. Express 8 (2018) 2722.

[9] M. Kang, A.M. Swisher, A.V. Pogrebnyakov, L. Liu, A. Kirk, S. Aiken, L. Sisken, C. Lonergan, J. Cook, T. Malendevych, F. Kompan, I. Divliansky, L.B. Glebov, M.C. Richardson, C. Rivero-Baleine, C.G. Pantano, T.S. Mayer, K. Richardson, Ultra-low dispersion multicomponent thin film chalcogenide glass for broadband gradient index optics, Adv. Mater. 30 (2018) 1803628.

[10] L. Sisken, C. Smith, A. Buff, M. Kang, K. Chamma, P. Wachtel, J.D. Musgraves, C. Rivero-Baleine, A. Kirk, M. Kalinowski, M. Melvin, K. Richardson, Evidence of spatially selective refractive index modification in 15GeSe$_2$-45As$_2$Se$_3$-40PbSe glass through correlation of structure and optical property measurements for GRIN applications, Opt. Mater. Exp. 7 (2017) 3077.

[11] L. Sisken, M. Kang, J.M. Veras, C. Lonergan, A. Buff, A. Yadav, D. McClane, C. Blanco, C. Rivero-Baleine, T.S. Mayer, K.A. Richardson, Infrared glass-ceramics with multidispersion and gradient refractive index attributes, Adv. Funct. Mater. (2019) (in press).

[12] J. Hu, V. Tarasov, A. Agarwal, L. Kimerling, N. Carlie, L. Petit, K. Richardson, Fabrication and testing of planar chalcogenide waveguide integrated microfluidic sensor, Opt. Express 15 (2007) 2307.

[13] J. Wang, J. Hu, X. Sun, A.M. Agarwal, L.C. Kimerling, D.R. Lim, R.A. Synowicki, Structural, electrical, and optical properties of thermally evaporated nanocrystalline PbTe films, J. Appl. Phys. 104 (2008) 053707.

[14] C. Gaida, M. Gebhardt, P. Kadwani, L. Leick, J. Broeng, L. Shah, M. Richardson, Amplification of nanosecond pulses to megawatt peak power levels in Tm^{3+}-doped photonic crystal fiber rod, Opt. Lett. 38 (2013) 691.

[15] I. Mingareev, M. Kang, T. Malendevych, G. Yin, J. Hu, K. Richardson, M. Richardson, Laser-induced modification of local refractive index in infrared glass-ceramic films, Proc. SPIE 10906 (2019) 109060X.

[16] M. Kang, T. Malendevych, G. Yin, I.B. Murray, M.C. Richardson, J. Hu, I. Mingareev, K. Richardson, Scalable laser-written Ge-As-Pb-Se chalcogenide glass-ceramic films and the realization of infrared gradient refractive index elements, Proc. SPIE 10998 (2019) 109980E.

[17] M.F. Koldunov, A.A. Manenkov, I.L. Pocotilo, Multishot laser damage in transparent solids: theory of accumulation effect, Proc SPIE 2428 (1995) 653.

[18] J.-L. Adam, X. Zhang, Chalcogenide glasses: preparation, properties and applications, Woodhead publishing, 2014.

[19] I. Mingareev, M. Ramme, M. Richardson, Material response of semiconductors irradiated with IR ultrashort laser pulses, Proc. CLEO-PR 2 (2015) 1–2.

[20] I. Mingareev, N. Gehlich, T. Bonhoff, A. Abdulfattah, A.M. Sincore, P. Kadwani, L. Shah, M. Richardson, Principles and applications of trans-wafer processing using a 2-μm thulium fiber laser, Int. J. Adv. Manuf. Technol. 84 (2016) 2567–2578.

[21] Mingareev, I. 2019, unpublished work.

[22] M. Kang, J. Qin, M. Truman, C.M. Schwarz, I.B. Murray, M.C. Richardson, J. Hu, I. Mingareev, K.A. Richardson, A roadmap for scalable refractive index design and fabrication in broadband infrared glass-ceramic films, 2019 (in preparation).